

Calorons and Localization of Quark Eigenvectors in Lattice QCD

M. Göckeler,¹ P. E. L. Rakow,¹ A. Schäfer,¹ W. Söldner,¹ and T. Wettig^{2,3}

¹*Institut für Theoretische Physik, Universität Regensburg, D-93040 Regensburg, Germany*

²*Center for Theoretical Physics, Yale University, New Haven, Connecticut 06520-8120*

³*RIKEN BNL Research Center, Brookhaven National Laboratory, Upton, New York 11973-5000*

(Received 3 April 2001; published 6 July 2001)

We analyze the localization properties for eigenvectors of the Dirac operator in quenched lattice QCD in the vicinity of the deconfinement phase transition. Studying the characteristic differences between the Z_3 sectors above the critical temperature T_c , we find indications for the presence of calorons.

DOI: 10.1103/PhysRevLett.87.042001

PACS numbers: 12.38.Gc, 11.15.Ha, 11.30.Rd

One of the most discussed topics in hadron physics is the chiral phase transition of QCD, and the microscopic processes connected with it. Many current and planned experiments are at least partially motivated by the hope that they will shed some light on the issues involved.

In this Letter we study the localization properties of the lattice Dirac operator in the neighborhood of the chiral phase transition. We are motivated by the fact that one of the most popular pictures of the phase transition relates it to the properties of QCD instantons and anti-instantons (see, e.g., Ref. [1]). The origin of this connection is the following observation: For each isolated instanton or anti-instanton there exists a localized zero mode of the Dirac operator. For a liquid of instantons and anti-instantons these zero modes should be perturbed to form a band of small eigenvalues. At higher temperatures it is thought that instantons and anti-instantons may pair to form molecules, and that the associated modes will no longer have particularly small eigenvalues, but instead become an inconspicuous part of the bulk spectrum.

The Banks-Casher formula [2],

$$\langle \bar{q}q \rangle = -\frac{\pi \rho_{\text{Dirac}}(0)}{V}, \quad (1)$$

relates the chiral condensate $\langle \bar{q}q \rangle$ to $\rho_{\text{Dirac}}(0)$, the density of Dirac eigenvalues at zero, evaluated in the (large) volume V . Thus we expect that if the instantons and anti-instantons form a liquid, chiral symmetry will be broken, but that if they form instanton-anti-instanton molecules, chiral symmetry will be restored.

If this interpretation is correct, the chiral phase transition should reflect itself also in a characteristic change of the localization properties of the lowest Dirac eigenvectors. This is the main motivation for our studies.

In addition, we are interested in comparing our lattice results with predictions from random matrix theory (RMT). Such a comparison allows us to distinguish generic from QCD-specific properties. Similar studies were performed before in Ref. [3]. In this paper, however, the authors analyzed a specific instanton-liquid approximation to QCD while we study lattice QCD.

As usual, we simulate a finite-temperature system by working on a lattice with $L_t < L_s$, where L_t (L_s) is the

temporal (spatial) extent of the lattice. All boundary conditions are periodic except for the temporal boundary conditions of the fermions which are antiperiodic. The temperature is given by $aT = 1/L_t$ with the lattice spacing a . We fix $L_t = 6$ and vary a (and hence T) by changing $\beta = 6/g^2$.

We work in the quenched approximation with staggered fermions, i.e., with the Dirac operator

$$D = \sum_{\mu=1}^4 \frac{1}{2a} \alpha_{\mu}(x) [\delta_{y,x+\hat{\mu}} U_{\mu}(x) - \delta_{y,x-\hat{\mu}} U_{\mu}^{\dagger}(y)], \quad (2)$$

where $\alpha_{\mu}(x) = (-1)^{x_1+\dots+x_{\mu-1}}$ and the U_{μ} are the link variables. The eigenvalues of D come in pairs of $\pm i\lambda$ with λ real, so we can restrict ourselves to positive λ in the following. In the continuum limit this action corresponds to four quark flavors. From now on we set a to 1.

Quenched QCD has an additional Z_3 symmetry of the gauge sector, which is spontaneously broken in the deconfined phase [4]. In the confined phase the expectation value of the Polyakov loop P is zero, whereas in the deconfined phase $|P|$ acquires an expectation value, and the phase of P clusters around the values $\theta_P = \arg(P) = 0, \pm 2\pi/3$. The fermion action does not share the Z_3 symmetry, so fermionic quantities can depend on the Z_3 sector. It was found in Ref. [5] that the chiral condensate computed from the configurations with $\theta_P = 0$ vanishes above T_c as expected. For $\theta_P = \pm 2\pi/3$ it remains finite in a certain temperature range above T_c . This behavior can be understood in Nambu-Jona-Lasinio models [6,7] and in RMT [8]. The point is that the boundary conditions of the Dirac operator are not invariant under Z_3 transformations, and for $\theta_P = \pm 2\pi/3$ the new boundary conditions lead to a decrease of the Dirac eigenvalues [8]. According to the Banks-Casher relation, Eq. (1), this implies that the condensate will disappear only for larger temperatures, i.e., the transition temperature is higher for these sectors. For phenomenological comparisons one should use the $\theta_P = 0$ sector as this one is energetically favored for dynamical fermions. (The sectors $\theta_P = \pm 2\pi/3$ are physically equivalent to each other.) We refer to the $\theta_P = 0$ sector as the real sector and to the $\theta_P = \pm 2\pi/3$ sectors as the complex sector.

Large temperatures correspond to a small extension of the lattice in the temporal direction. The periodic boundary conditions for the gauge fields thus imply that the field equations have solutions with nontrivial topology which look rather like an instanton chain [9]. Such configurations, called calorons, have been the topic of intense investigations [1].

The index theorem tells us that the continuum Dirac operator has a chiral zero mode in a caloron field, so we will search for calorons by looking at the chiral and localization properties of the eigenvectors of the low-lying eigenvalues of D . To calculate the eigenvalues and eigenvectors we used the Arnoldi method as implemented in Ref. [10]. This method allows us to choose the number of the lowest eigenvalues and eigenvectors to be calculated.

In the continuum a zero mode has a definite chirality (= expectation value $\langle\gamma_5\rangle$) of ± 1 , while modes with $\lambda \neq 0$ have $\langle\gamma_5\rangle = 0$. Staggered fermions possess only a restricted chiral symmetry, so in this case we expect $\langle\gamma_5\rangle$ values between -1 and 1 . In Fig. 1 we show a scatter plot of $\langle\gamma_5\rangle$ against Dirac eigenvalue, for a temperature slightly above T_c . We can see that in all sectors the data points form clusters. There are some eigenmodes with very small eigenvalue, and $\langle\gamma_5\rangle \approx \pm 0.2$, while the bulk of the eigenvectors have a larger λ , and $\langle\gamma_5\rangle$ near zero. The modes labeled 1 to 3 in Figs. 1 and 2 will be discussed below.

A large value of $\langle\gamma_5\rangle$ suggests that the corresponding eigenvectors have a topological origin, in which case they should be associated with specific localized states. This interpretation is supported by the fact that these modes are approximately fourfold degenerate as they should be because of the flavor symmetry of staggered fermions in the continuum limit. One of our main results is that these states may be important for understanding the differences between the Z_3 sectors.

As a measure of the localization of our quark eigenvectors $\psi_\lambda^\alpha(x)$ (λ is the Dirac eigenvalue, α a color index) we

use a gauge-invariant inverse participation ratio (IPR), defined by

$$I_2 \equiv V \frac{\sum_x p_\lambda(x)^2}{[\sum_x p_\lambda(x)]^2}, \quad (3)$$

where V is the number of lattice sites and $p_\lambda(x)$ is the gauge-invariant probability density

$$p_\lambda(x) = \sum_{\alpha=1}^{N_c} |\psi_\lambda^\alpha(x)|^2. \quad (4)$$

For a completely delocalized state [all $p_\lambda(x)$ the same] one finds $I_2 = 1$, whereas a state localized on a single lattice site [only one nonzero $p_\lambda(x)$] would have $I_2 = V$. (The staggered fermions' chiral symmetry means that, in fact, an eigenstate can never be completely localized, since all eigenstates must have half their probability on even sites, and half on odd.) I_2 is also a measure of the standard deviation of $p_\lambda(x)$,

$$I_2 - 1 = \frac{\sum_x [p_\lambda(x) - \bar{p}_\lambda]^2}{V \bar{p}_\lambda^2}. \quad (5)$$

Chiral RMT predicts that the average value of I_2 is

$$\langle I_2 \rangle = \frac{(N_c + 1)V}{N_c V + 2} \xrightarrow{V \rightarrow \infty} 1 + \frac{1}{N_c} \quad \text{for } N_c \geq 3. \quad (6)$$

To elucidate the relevance of the IPR let us note that in condensed matter physics the size of the IPR decides, e.g., whether a disordered mesoscopic sample is a metal (I_2 close to the RMT prediction) or an insulator (I_2 large).

We have investigated the behavior of I_2 on finite temperature lattices, on both sides of the deconfinement phase transition, which lies at $\beta \approx 5.89$ for $L_t = 6$ in the thermodynamic limit [11].

Slightly above T_c the localization properties show characteristic differences for the different Z_3 sectors. In the real sector the effect of localization is strongly pronounced while it is nearly absent in the $\theta_P = \pm 2\pi/3$ sectors. This is illustrated in Figs. 2 and 3 in which we divided the ensembles of gauge configurations into configurations with

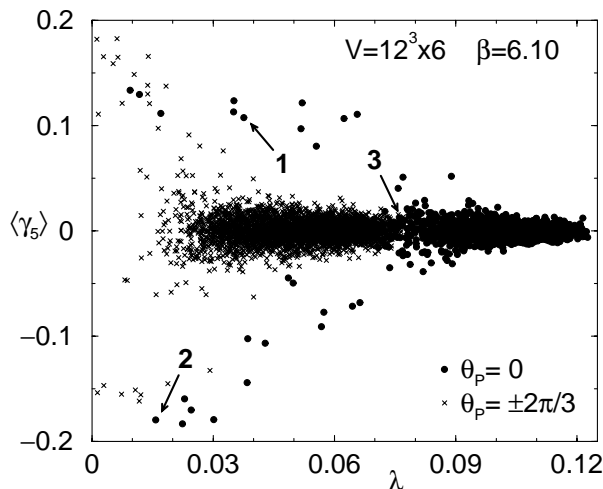


FIG. 1. $\langle\gamma_5\rangle$ vs λ . The measurements are on a $12^3 \times 6$ lattice at $\beta = 6.10$ for both sectors, $\theta_P = 0$ and $\theta_P = \pm 2\pi/3$.

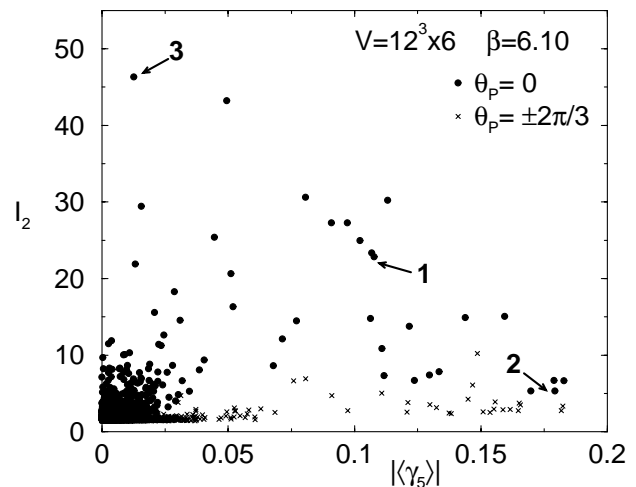


FIG. 2. A scatter plot of the localization vs chirality.

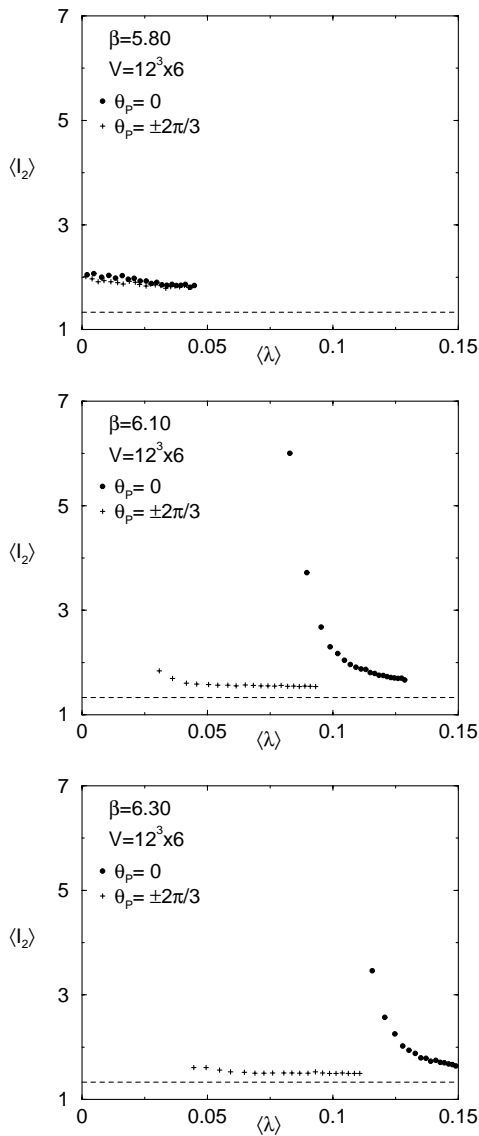


FIG. 3. From top to bottom, the average IPR for temperatures below, slightly above, and well above the chiral phase transition plotted separately for the Z_3 sector with $\theta_P = 0$ and the Z_3 sectors with $\theta_P = \pm 2\pi/3$. The average was performed for the 1st, 2nd, \dots , 20th eigenvalue of each gauge field configuration. The dashed line is the RMT prediction, $4/3$.

$-\pi/3 \leq \theta_P < \pi/3$ (real sector) and all other configurations (complex sector). A difference between localization in the different sectors tells us immediately that the eigenstates must be extended in the time direction, because an eigenstate localized in time would be unaffected by a Z_3 transformation. Naturally, we do not expect any differences in the localization properties for the different sectors when $T < T_c$.

We studied these characteristic differences for high temperatures in more detail and found features which suggest that they can be attributed to the effects of calorons, as we shall now explain.

Harrington and Shepard found exact $SU(2)$ instanton solutions at finite temperature [9], which they called calorons

(for a review see Ref. [12]). Their solution consists of a one-dimensional chain of instantons, with a periodic repeat at a distance $1/T$. There is a single physically relevant parameter, RT , which gives the instanton radius R , relative to the scale set by the temperature. When $RT \ll 1$ the solution looks like an isolated instanton, but when $RT \sim 1$ finite temperature effects become significant. This instanton chain satisfies the 't Hooft ansatz [13], so the techniques described in Ref. [14] can be used to find the fermionic zero modes [15]. For small RT these look like the zero modes of an isolated instanton, but as RT increases, the modes become extended in time, though they remain localized in space. These $SU(2)$ solutions can easily be embedded in $SU(3)$, leading to solutions which correspond to the $\theta_P = 0$ sector. To investigate the other sectors, we need solutions where the timelike Polyakov loop has a nonzero phase at spacelike infinity. We can construct such solutions either by adding a constant A_4 background field with a color that commutes with the $SU(2)$ subgroup containing the caloron, or by choosing the fermion field boundary condition appropriately. In either case the fermionic zero modes are readily constructed. One can also find pure $SU(2)$ solutions with a Polyakov loop background [16]. It would be interesting to study the relationship between these solutions and the solutions found by embedding the Harrington-Shepard solution in $SU(3)$.

The localization of the embedded caloron's fermion zero mode depends heavily on the Z_3 sector. Asymptotically the modes fall off like

$$|\psi|^2 \propto \exp[-2(\pi - |\theta_P|)rT]/r^2, \quad (7)$$

where r is the three-dimensional distance from the caloron axis. (At $\theta_P = 0$, this agrees with the behavior given in Ref. [12].) This is unlike the case of a single instanton, which has $|\psi|^2$ which drops off like a power of r . We see from Eq. (7) that the correlation length for the zero mode is smallest in the real sector ($\theta_P = 0$), and that the complex Z_3 sectors ($\theta_P = \pm 2\pi/3$) have modes in which the radius is about 3 times greater, and so they occupy a much larger volume. It is thus tempting to assume that the strong difference between the localization properties in the Z_3 sectors is due to the fact that our lattice configurations contain calorons. If so, the localization in four dimensions should show the characteristic stringlike pattern discussed above.

In Fig. 4 the localization itself and the local density of the expectation value of γ_5 are shown for a highly localized state in the $\theta_P = 0$ sector (mode 1 of Figs. 1 and 2). To plot the complete four-dimensional lattice we have introduced the two coordinates $i = x + 12t$ and $j = y + 12z$ with the Euclidean lattice coordinates $x, y, z = 0, 1, 2, \dots, 11$ and $t = 0, \dots, 5$. This coordinate system represents the lattice as a 6×12 array of x - y slices, which generates the approximately periodic structure visible in the plot. From the upper plot, we see that the state is indeed

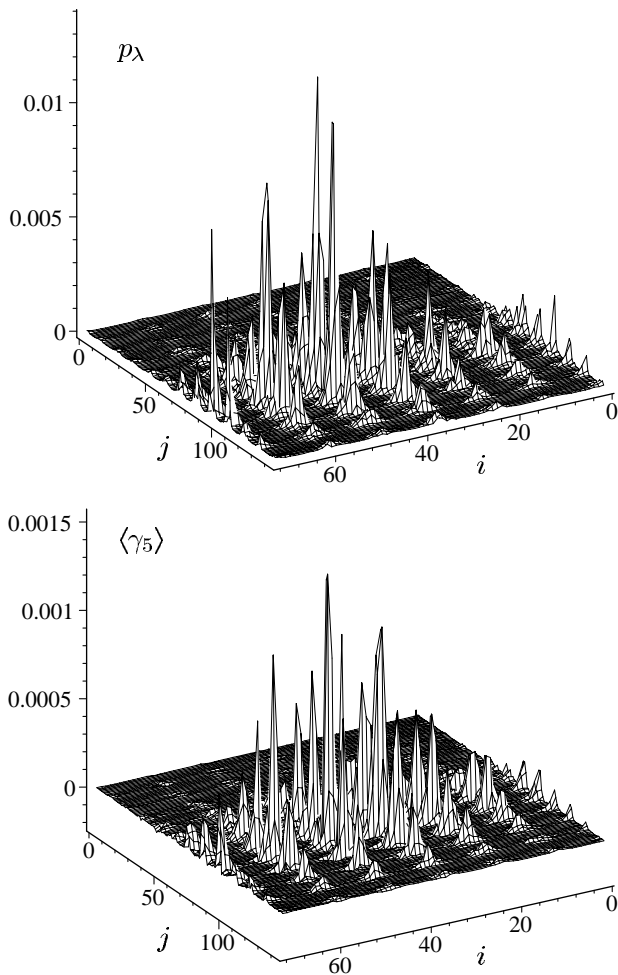


FIG. 4. A “caloron” state (mode 1 of Figs. 1 and 2) on a $12^3 \times 6$ lattice for $\beta = 6.1$ in the $\theta_p = 0$ sector. We have introduced the coordinates $i = x + 12t$ and $j = y + 12z$ with the lattice coordinates $x, y, z = 0, 1, \dots, 11$ and $t = 0, \dots, 5$. The gauge-invariant density is plotted above, the expectation value of γ_5 below. Both show localization in space but not in time.

spatially localized, but extended in time. The lower plot demonstrates that the eigenstate in question is an approximate chiral eigenstate. A continuum caloron would possess an exact chiral eigenstate. Unfortunately, staggered fermions exhibit only part of the continuum chiral symmetry, which is the reason why we do not find perfect γ_5 eigenstates. It would therefore be very interesting to repeat these studies with Ginsparg-Wilson fermions which have much better chiral properties.

The corresponding pictures for mode 2 look similar to Fig. 4. The width of the mode is, however, noticeably larger than that of mode 1. Mode 3 serves as an example for a mode with low $\langle \gamma_5 \rangle$, high I_2 , and an eigenvalue which lies in the bulk of the spectrum. Although $\langle \gamma_5 \rangle$ is small, the $\langle \gamma_5 \rangle$ density has a region of large positive values right next to a region where the density is large and negative.

This suggests mode 3 might be an instanton–anti-instanton molecule.

Modes related to instantons and calorons were recently investigated in lattice QCD with dynamical fermions [17]. While the results below T_c are consistent with expectations based on an instanton liquid picture, the interpretation of the observations above T_c appears to be less straightforward.

To summarize, we have analyzed the localization properties of quark eigenstates in quenched lattice QCD. By concentrating on the low eigenvalues we could characterize semiclassical properties of the gauge field configurations without any cooling. (For investigations using cooling, see, e.g., Refs. [18,19].) For temperatures above T_c we found isolated modes with definite handedness which show all the properties of fermion states associated with calorons, in particular localization in space but not in time.

We thank A. V. Belitsky, Ph. de Forcrand, and T. Schäfer for useful conversations.

-
- [1] E.-M. Ilgenfritz and E. V. Shuryak, Phys. Lett. B **325**, 263 (1994); T. Schäfer and E. V. Shuryak, Rev. Mod. Phys. **70**, 323 (1998); R. Rapp, T. Schäfer, E. V. Shuryak, and M. Velkovsky, Ann. Phys. (N.Y.) **280**, 35 (2000).
 - [2] T. Banks and A. Casher, Nucl. Phys. **B169**, 103 (1980).
 - [3] J. C. Osborn and J. J. M. Verbaarschot, Phys. Rev. Lett. **81**, 268 (1998); Nucl. Phys. **B525**, 738 (1998).
 - [4] A. M. Polyakov, Phys. Lett. **72B**, 477 (1978); B. Svetitsky and L. G. Yaffe, Nucl. Phys. **B210** [FS6], 423 (1982).
 - [5] S. Chandrasekharan and N. H. Christ, Nucl. Phys. B (Proc. Suppl.) **47**, 527 (1996).
 - [6] P. N. Meisinger and M. C. Ogilvie, Phys. Lett. B **379**, 163 (1996).
 - [7] S. Chandrasekharan and S. Huang, Phys. Rev. D **53**, 5100 (1996).
 - [8] M. A. Stephanov, Phys. Lett. B **375**, 249 (1996).
 - [9] B. J. Harrington and H. K. Shepard, Phys. Rev. D **17**, 2122 (1978); **18**, 2990 (1978).
 - [10] <http://www.caam.rice.edu/software/ARPACK/>
 - [11] G. Boyd *et al.*, Nucl. Phys. **B469**, 419 (1996).
 - [12] D. J. Gross, R. D. Pisarski, and L. G. Yaffe, Rev. Mod. Phys. **53**, 43 (1981).
 - [13] G. 't Hooft (unpublished); R. Jackiw, C. Nohl, and C. Rebbi, Phys. Rev. D **15**, 1642 (1977).
 - [14] B. Grossman, Phys. Lett. **61A**, 86 (1977); H. Osborn, Nucl. Phys. **B140**, 45 (1978).
 - [15] N. Bilić, Phys. Lett. **97B**, 107 (1980).
 - [16] T. C. Kraan and P. van Baal, Nucl. Phys. **B533**, 627 (1998); Phys. Lett. B **428**, 268 (1998); K. Y. Lee and C. Lu, Phys. Rev. D **58**, 025011 (1998).
 - [17] Ph. de Forcrand *et al.*, Nucl. Phys. B (Proc. Suppl.) **73**, 578 (1999); hep-lat/9802017.
 - [18] M. L. Laursen and G. Schierholz, Z. Phys. C **38**, 501 (1988); E.-M. Ilgenfritz *et al.*, hep-lat/0011051.
 - [19] S. Hands, Nucl. Phys. **B329**, 205 (1990).